Soft Matter

Reaction-induced morphological transitions in a blend of diblock copolymer and reactive monomer: dissipative particle dynamics simulation

Journal:	*Soft Matter*
Manuscript ID	SM-ART-07-2023-000959.R1
Article Type:	Paper
Date Submitted by the Author:	17-Nov-2023
Complete List of Authors:	Tomiyoshi, Yoshinori; Ochanomizu University, Oya, Yutaka; Tokyo University of Science - Katsushika Campus Kawakatsu, Toshihiro; Tohoku University, Department of Physics Okabe, Tomonaga; Tohoku University Graduate School of Engineering School of Engineering Department of Mechanical and Aerospace Engineering

SCHOLARONE™
Manuscripts

Soft Matter

ARTICLE TYPE

Cite this: DOI: 00.0000/xxxxxxxxxx

Reaction-induced morphological transitions in a blend of diblock copolymer and reactive monomer: dissipative particle dynamics simulation†

Yoshinori Tomiyoshi,*[a] Yutaka Oya,[b] Toshihiro Kawakatsu[c] and Tomonaga Okabe[d]

Received Date
Accepted Date

DOI: 00.0000/xxxxxxxxxx

Dissipative particle dynamics (DPD) method is applied to the morphological transitions of microphase-separated domains in a mixture of symmetric AB-diblock copolymer and reactive C-monomer, where polymerization and cross-linking reactions take place among C-monomers. The initial structure for the DPD simulation is an equilibrated cylindrical domain structure prepared by the density-biased Monte Carlo method with density profiles obtained from the self-consistent field theory. By introducing a cross-linking reaction among reactive C-monomers, we confirmed that the DPD simulation reproduces the morphological transitions observed in experiments, where the domain morphology changes due to a segregation between A-block of diblock copolymers and cross-linking networks of C-monomers. When the cross-linking reaction of C-monomers is sufficiently fast compared to the deformation of the domains, the initial cylindrical domains are preserved, while the distance between the domains increases. On the other hand, when the formation of the cross-linking network is slow, the domains can deform and reconnect with each other in the developing cross-linking network. In this case, we observe morphological transitions from the initial domain morphology with a large-curvature interface to another domain morphology with a smaller-curvature interface, such as the transition from the cylindrical phase to the lamellar phase. We calculated the spatial correlations in the microphase-separated domains and found that such correlations are affected by the speed of the formation of the cross-linking network depending on whether the bridging between microphase-separated domains occurs in a nucleation and growth process or in a spinodal decomposition process.

1 Introduction

Controlling properties of polymeric materials by blending polymers is of crucial importance in designing various composites. One of the successful examples is a thermosetting/thermoplastic polymer blend [1–3]. Epoxy resins have been widely used for industrial products including electronic and adhesive materials [4,5] and fiber-reinforced composites like CFRP (Carbon-Fiber-Reinforced Plastics) [6,7] because the epoxy resins have desirable mechanical and physical characteristics such as high thermal conductivity and insulation, except its toughness. It is well known that while epoxy resins possess large rigidity for many engineering applications, they allow cracks to grow and to propagate easily, which leads to their undesirable brittleness. To overcome this brittleness of the epoxy resins, block copolymers have attracted a great attention as a thermoplastic modifier to control the structure of nanoscale domains by their self-assembly [8–12]. The improvement of the fracture toughness has been observed in the experiments. Wu *et al.* [8] reported that in the blend of epoxy and PBO–PEO (polybutylene oxide-b-ethylene oxide), the microphase-separated structure of branched worm-like micelles shows 19 times strain energy release rate, which characterizes the toughness, than the unmodified epoxy without the PBO-PEO. Kishi *et al.* [11] also reported that in epoxy/acrylic block copolymers (PMMA-b-PnBA-b-PMMA, poly(methyl methacrylate)-b-poly(n-butyl acrylate)-b-poly(methyl metacrylate)), the nano-cylindrical structures have the 2530 J/m^2 as the fracture toughness, which is twenty-fold compared to the unmodified epoxy thermosets. These observations undoubtedly indicate the importance of the precise prediction of the microphase-separated structures with curing or

[a] Center for Soft Matter Physics, Ochanomizu University, Bunkyo-ku, Tokyo 112-8610, Japan; E-mail: tomiyoshi.yoshinori@ocha.ac.jp
[b] Department of Materials Science and Technology, Tokyo University of Science, Katsushika-Ku, 125-8585, Tokyo, Japan
[c] Department of Physics, Graduate School of Science, Tohoku University, Sendai 980-8578, Japan
[d] Department of Aerospace Engineering, Graduate School of Engineering, Tohoku University, Sendai 980-8578, Japan

† Electronic Supplementary Information (ESI) available: movies of the morphological transitions under the cross-linking reaction discussed in Section 4.1. See DOI: 10.1039/cXsm00000x/

cross-linking reactions to improve the functionalities of the epoxy resins.

To understand the mechanism of the microphase-separated structures of the epoxy/block copolymer blend, we focus on a pioneering experimental works reported by Lipic *et al.* [13,14]. Their study employed a sample containing Poly(ethylene oxide)-b-poly(ethyl ethylene-*alt*-propylene) (PEO-PEP) modifiers added to the diglycidyl ether of bisphenol-A (DGEBA) type epoxy thermosets. The authors reported that, depending on the volume fraction of modifiers and the temperature, the epoxy/block copolymer blend formed the microphase-separated structures such as lamellar, gyroid, hexagonal cylinder, and spheres before curing reaction. During the curing reaction, these microphase-separated structures transform into different morphologies, e.g., from sphere into cylinder. Their study demonstrates that "reaction-induced phase separation"[15,16] plays an important role in these morphological transitions.

As far as we know, few works have been paid attention to reaction-induced morphological transitions for microphase-separated structures in view of the particle-based simulation, although several works studied reaction-induced "macrophase" separations[17–20]. In the present paper, by using dissipative particle dynamics (DPD) with a simple cross-linking reaction scheme, we simulate the epoxy/block copolymer blend in the mesoscopic scale. To simply mimic the target system studied by Lipic *et al.*[14], we investigate the morphological transitions in a blend of AB-diblock copolymers and reactive C-monomers, as we will explain in the next section. We first perform self-consistent field theory (SCFT) calculation to confirm the phase diagram obtained in the experiment. With the aid of the density profile of microphase-separated structures obtained from SCFT, we prepare well-ordered initial conditions for efficient DPD simulations. Starting from these initial conditions, we simulate the reaction-induced morphological transitions induced by the cross-linking reaction of reactive monomers. We also investigate the transient dynamics of the morphological transitions for various cross-linking conditions.

2 Model and simulation

To simulate our target system studied by Lipic *et al.*[14] in the mesoscopic scale, we employ the standard DPD method[21,22] and we assume that our system consists of three types of DPD particles: A and B particles in the symmetric diblock copolymers (PEO-PEP) and reactive C particles (epoxy) as a reactive solvent monomer as shown in Fig. 1. The reactive C particle forms a cross-linking network structure. We assume that the mixing of A particles in the diblock copolymer and the reactive C particles is athermal.

In the following, we briefly review the DPD method used in the present paper. This method has been applied to predict the kinetics of microphase separations of diblock copolymers[23], and has recently been used for modeling polymer networks[24,25] and a thermoset resin curing simulation[26]. The motion of the DPD particles is described by Newton's equations of motion

$$\frac{d\mathbf{r}_i}{dt} = \mathbf{v}_i, \quad m\frac{d\mathbf{v}_i}{dt} = \mathbf{F}_i, \tag{1}$$

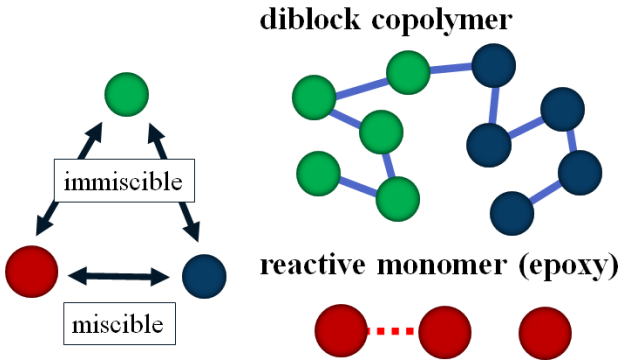

Fig. 1 Schematic picture of the model used in this study. Symmetric diblock copolymers are modeled by five A (blue) particles and five B (green) particles, which have a repulsive interaction with each other. Reactive C (red) particles are immiscible with B particles, and they can react to form the cross-linking networks.

where t is time, m the mass of a DPD particle, $\mathbf{v}_i$ the velocity of i-th particle, and $\mathbf{F}_i$ the total force acting on i-th particle. The total force $\mathbf{F}_i$ consists of four contributions:

$$\mathbf{F}_i = \sum_{j(\neq i)} \left(\mathbf{F}_{ij}^{\mathrm{C}} + \mathbf{F}_{ij}^{\mathrm{D}} + \mathbf{F}_{ij}^{\mathrm{R}} + \mathbf{F}_{ij}^{\mathrm{B}}\right), \tag{2}$$

where $\mathbf{F}_{ij}^{\mathrm{C}}$ is a conservative force from j-th particle acting on i-th particle, $\mathbf{F}_{ij}^{\mathrm{D}}$ a dissipative force, $\mathbf{F}_{ij}^{\mathrm{R}}$ a random force, and $\mathbf{F}_{ij}^{\mathrm{B}}$ a spring force which connects neighboring particles along the chain. The dissipative and random forces are given by

$$\mathbf{F}_{ij}^{\mathrm{D}} = -\gamma\omega^{\mathrm{D}}(|\mathbf{r}_{ij}|)(\hat{\mathbf{r}}_{ij}\cdot\mathbf{v}_{ij})\hat{\mathbf{r}}_{ij} \tag{3}$$

and

$$\mathbf{F}_{ij}^{\mathrm{R}} = \sigma\omega^{\mathrm{R}}(|\mathbf{r}_{ij}|)\theta_{ij}(t)\hat{\mathbf{r}}_{ij}, \tag{4}$$

where $\mathbf{r}_{ij} \equiv \mathbf{r}_i - \mathbf{r}_j$, $\hat{\mathbf{r}}_{ij} = \mathbf{r}_{ij}/|\mathbf{r}_{ij}|$, and $\mathbf{v}_{ij} \equiv \mathbf{v}_i - \mathbf{v}_j$. γ is a friction coefficient and σ a noise strength which satisfies the fluctuation-dissipation theorem $\sigma^2 = 2\gamma k_{\mathrm{B}}T$, θ_{ij} a Gaussian white noise characterized by

$$\langle\theta_{ij}(t)\rangle = 0, \tag{5}$$

$$\langle\theta_{ij}(t)\theta_{kl}(t')\rangle = (\delta_{ik}\delta_{jl} + \delta_{il}\delta_{jk})\delta(t-t'), \tag{6}$$

and ω^{D} and ω^{R} are the weighting functions proposed by Español and Warren[23] as:

$$\omega^{\mathrm{D}}(|\mathbf{r}_{ij}|) = [\omega^{\mathrm{R}}(|\mathbf{r}_{ij}|)]^2 = \begin{cases} (1-|\mathbf{r}_{ij}|)^2, & (|\mathbf{r}_{ij}| < r_c) \\ 0. & (|\mathbf{r}_{ij}| \geq r_c), \end{cases} \tag{7}$$

where r_c is the cutoff radius.

As the conservative force, we adopt the soft repulsion force defined by

$$\mathbf{F}_{ij}^{\mathrm{C}} = \begin{cases} a_{ij}\left(1-|\mathbf{r}_{ij}|/r_c\right)\hat{\mathbf{r}}_{ij}, & |\mathbf{r}_{ij}| < r_c \\ 0 & |\mathbf{r}_{ij}| \geq r_c, \end{cases} \tag{8}$$

where a_{ij} is a repulsive interaction between i-th and j-th particles. In this paper, a_{ij}'s are determined according to the study by Groot and Warren[22], where the repulsive interaction between the same types of particles a_{ii} is determined by

$$a_{ii} = 75 k_B T / \rho, \tag{9}$$

where ρ is the mean particle number density, and the interaction between the different types of particles a_{ij} is determined by

$$a_{ij} = a_{ii} + 3.27\chi_{ij} \tag{10}$$

for $\rho = 3$, where χ_{ij} is the Flory-Huggins χ-parameter. To construct bead-spring chains by the DPD particles, we introduce the linear spring between bonded particles,

$$\mathbf{F}^{\mathrm{B}}_{ij} = k\mathbf{r}_{ij}, \tag{11}$$

where k is the spring constant.

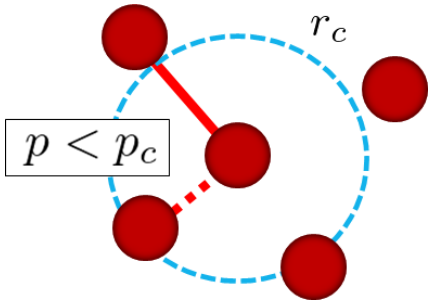

Fig. 2 Schematic picture of the cross-linking reaction in this simulation. r_c is the cutoff radius of the monomer, within which the possible candidates for the cross-linking reactions are searched for. When a uniform random number p is smaller than a threshold value p_c, i.e., $p < p_c$, we assign a linear spring as a cross-linking bond between these monomers.

In addition to the standard DPD methodology explained above, we introduce a simple reaction algorithm for the stochastic bond creation to reproduce the cross-linking process of reactive monomers. The reaction procedure is as follows:

1. For each reactive monomer, we list up surrounding reactive monomers within a given distance r_c.
2. We randomly choose one reactive monomer from the surrounding monomers listed up in step 1.
3. We create a permanent chemical bond between these monomers when $p < p_c$ where p is a uniform random number in [0,1].

In this study, each reactive monomer can have up to 4 bonds. The above procedure is applied at every μ DPD time steps and for all monomers except those with 4 bonds. Fig. 2 shows a schematic picture of the cross-linking reaction in this simulation explained above. A similar method for the cross-linking reaction was used in Refs[17,24].

Before starting DPD simulations, we apply the SCFT for investigating the possible microphase-separated structures depending on the volume fraction of A segment and the repulsive interaction between segments, and also apply the density-biased Monte Carlo method[27] for preparing well-ordered microphase-separated structures as initial conditions for DPD simulations. We use COGNAC and SUSHI in OCTA[28] as the DPD simulator and the SCFT simulator, respectively. About the theoretical details of SCFT and the density-biased Monte Carlo method, readers can refer to Refs.[27,29].

3 Equilibrium microphase-separated structures before curing reactions

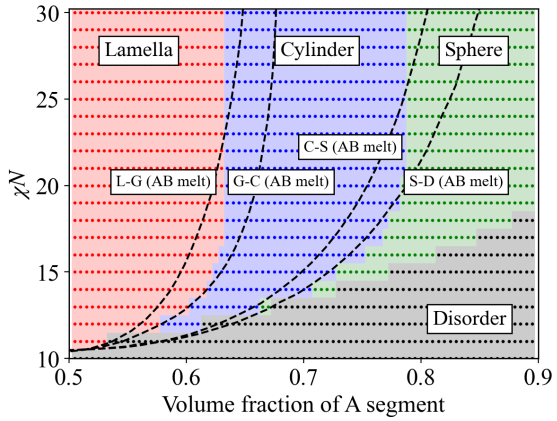

Fig. 3 Phase diagram obtained using SCFT. The horizontal axis represents the volume fraction of A segment for AB-diblock copolymer melts, and the total volume fraction of A segments and C segments for a blend of AB diblock polymer and C homopolymer. The dotted regions colored by red, blue, green, and gray represent lamellar, cylindrical, spherical, and disordered phases of the blend, respectively. We do not consider the gyroid morphology for simplicity in this study. Coexistence regions are omitted since these regions are too narrow to be shown. The dashed curves show the phase boundaries of the diblock copolymer melts between L-G, G–C, C–S, and S–D, where L, G, C, S, and D represent lamellar, gyroid, cylinder, sphere and disordered phases, respectively. These boundaries of the diblock copolymer melts are taken from Ref.[30]

In this section, we discuss the equilibrium microphase-separated structures in a blend of symmetric AB-diblock copolymer and C-homopolymer before the cross-linking reaction takes place. It should be noted that, in this section, we regard A and C monomers as the same species since their mixing is athermal. A theoretical phase diagram for such a blend of AB-diblock copolymer and A homopolymer system was obtained by Matsen[31,32] using SCFT. Semenov and Likhtman[33,34] also studied a similar system in the strong segregation regime by using the strong segregation theory (SST) for $N_{\mathrm{d}} < N_{\mathrm{h}}$, where N_{d} and N_{h} are the molecular weights of the diblock copolymer and the homopolymer, respectively. Here we investigate the system similar to these studies but $N_{\mathrm{d}} = 10$ and $N_{\mathrm{h}} = 1$, and focus on the weak and intermediate segregation regimes. The diblock copolymer with $N_{\mathrm{d}} = 10$ and reactive monomers with $N_{\mathrm{h}} = 1$ correspond to the PEO-PEP and epoxy (BPA348) in Ref.[14]. Since such a situation was not studied in Refs.[32–35], we newly constructed a phase diagram of the blend of AB-diblock copolymer and a homopolymer by using the SCFT, where the gyroid phase was not considered for simplicity as well as in our DPD simulations.

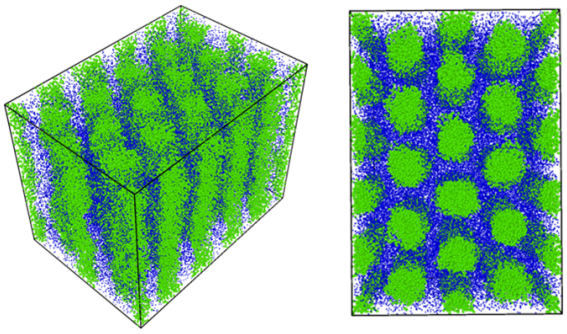

Fig. 4 The cylindrical phase as the initial condition for the DPD simulation obtained by the density-biased Monte Carlo method in Ref. [27]. Reactive C-monomers are not shown for visibility. We confirmed that these morphologies are stable in the simulation for 600,000 steps.

Figure 3 shows the phase diagram predicted by our SCFT calculation. Our phase diagram is qualitatively similar to the experimental result obtained by Lipic *et al.* [14]. It should be noted that in the intermediate regimes with $20 < \chi N < 30$, the location of the phase boundary between the lamellar and cylindrical phases and that between the cylindrical and spherical phases are independent of the incompatible parameter χN. Similar behavior is known to occur in the diblock copolymer melts (shown by the dashed curves in Fig. 3) but in a much stronger segregation region [36,37]. Moreover, the phase boundaries in the diblock copolymer and homopolymers blend locate at higher volume fraction regions than those in the diblock copolymer melts, since the homopolymers can fill the interstitial regions between the cylindrical or the spherical domains and relax the space-filling constraints imposed on the diblock copolymer melts. [33] We also note that the stable region of the spherical phase is much wider than the experimental result since the SCFT simulation does not include the thermal fluctuation effect which destabilizes the spherical phase. The density profile obtained by the SCFT simulation is used for efficiently generating the initial conditions of microscopic phase-separated structures for the DPD simulation by using the density-biased Monte Carlo method proposed in Ref. [27].

In the following sections, we show the results of the DPD simulation to investigate the effect of the cross-linking reaction on the initial domain morphologies. The total number of DPD particles are 139986, which are placed in a simulation box with $(L_x, L_y, L_z) = (44.0, 30.4, 34.9)$ for the cylindrical phase. A symmetric AB-diblock copolymer chain is composed of 5 A-particles and 5 B-particles, and thus a single block copolymer chain is composed of $N_\mathrm{d} = 10$ DPD particles. The total number density of the DPD particles is fixed to $\rho = 3$, and the total numbers of block copolymer chains and reactive C monomers are $(9797, 41998)$ which correspond to the number fraction of the A particles and C particles as $\phi_\mathrm{A} + \phi_\mathrm{C} = 0.65$. The interaction parameters between AA, BB, CC, and AC-type pairs are set to $a_\mathrm{AA} = a_\mathrm{BB} = a_\mathrm{CC} = a_\mathrm{AC} = 25$, while the interaction parameters for AB and BC-type pairs are set to $a_\mathrm{AB} = a_\mathrm{BC} = 46$, which corresponds to $\chi N = 64$ by Eq.(10). However, it should be noted that χN effectively reduces to $(\chi N)_\mathrm{eff} = 23 \sim 29$ by considering the fluctuation effect due to a finite chain length according to the following relations [23]:

$$(\chi N)_\mathrm{eff} = \frac{\chi N}{1 + 3.9 N^{-1/3}}, \tag{12}$$

or

$$(\chi N)_\mathrm{eff} = \frac{\chi N}{1 + 3.9 N^{-0.51}}. \tag{13}$$

Therefore, the condition of our DPD simulations in the next section corresponds to the intermediate segregation regime. As the parameters for the spring constant of the harmonic bond and the friction, $k = 4$ and $\sigma = 3.67$ are used [23]. The time integration of the equations of motion is done using a modified velocity-Verlet algorithm proposed by Groot and Warren [22] with time step $\delta t = 0.06$. We monitored the temperature during the cross-linking reactions and confirmed that the temperature is controlled within the acceptable range [22,23], even when we use $\delta t = 0.06$ with our reaction scheme. We performed three-dimensional DPD simulations starting from the initial conditions prepared in the above method. Figure 4 shows the cylindrical phase as the uncured initial condition for the DPD simulations. To realize a true equilibrium state, we set the system size to satisfy the isotropic pressure condition, $P_{xx} = P_{yy} = P_{zz}$, where $\mathbf{P}$ is pressure tensor. The same equilibrating procedure is used in Ref. [38]. It should be kept in mind that this condition is not useful for the spherical phase and the gyroid phase with the cubic symmetry, since the isotropic pressure is achieved even when the system size is not optimized.

4 Cross-linking reaction

In the following subsections, we show the dynamics of domains triggered by the reaction-induced phase separations during the cross-linking reactions among reactive C-monomers in our DPD simulation. For the case of the rapid reaction where the cross-linking reaction is so fast that the initial domains cannot deform, we show that the domain morphology is fixed as it was in the initial structure. On the other hand, for the slow reaction case where morphological domains can deform and reconnect with each other, the initial microphase-separated structure transforms into other structures depending on the degree of convergence of the cross-linking reaction. These dynamics are then further studied in detail.

4.1 Domain growth dynamics

According to Lipic *et al.* [14], the reaction-induced morphological transitions were experimentally observed for a mixture of PEO-PEP and epoxy (BPA348), and the mechanism of these transitions is explained in their paper as follows: In the initial equilibrium state, the PEO sub-chain of the diblock copolymer and the epoxy are miscible. When the cross-linking reaction occurs, the molecular weight of the epoxy networks becomes larger, which results in the decrease in the translational entropy of the epoxy molecules. This decrease of the translational entropy leads to the segregation between the PEO block and the epoxy network. At the same time, the curvature of the interface between PEO-PEP reduces since the effective volume fractions of PEO block swollen by the

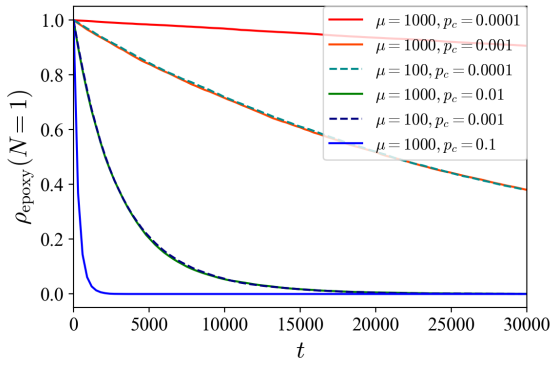

Fig. 5 The ratio of the number of unreacted C-monomers to the total number of C-monomers in the system as a function of time for several reaction conditions from the cylindrical phase as the initial state. In our simple reaction scheme, the decay rate of the number of unreacted monomers in the system depends on μ and p_c only through the product $\mu^{-1}p_c$.

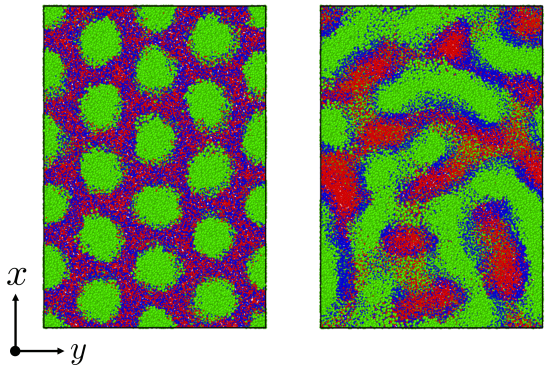

Fig. 6 The time evolution of the domain morphology starting from the cylindrical phase under the cross-linking reaction with the moderate reaction probability $p_c = 0.01$. (Left) $t = 0$, (Right) $t = 6000$. In these figures, only particles are visualized without bonds. To view the temporal evolutions of domain morphologies, see the movie in the supplemental material.

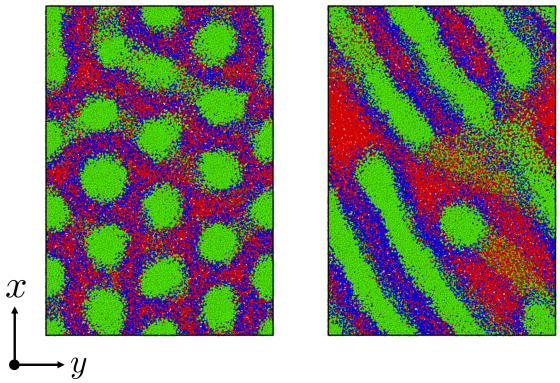

Fig. 7 Similar to Fig. 6 but with a low reaction probability $p_c = 0.0001$. (Left) $t = 26400$, (Right) $t = 48000$. To view the temporal evolutions of domain morphologies, see the movie in the supplemental material.

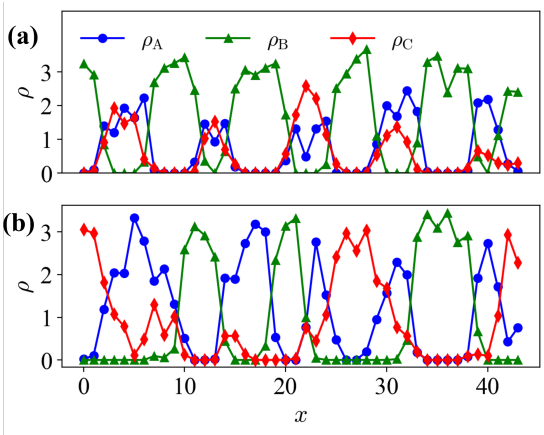

Fig. 8 Instantaneous one-dimensional density profile for each type of monomer along x-axis at $y = L_y/2$ and $z = L_z/2$. (a) Initial condition $t = 0$ (Fig.6(a)), and (b) $t = 48000$ for the case of $p_c = 0.0001$ (Fig. 7(b)).

epoxy decreases as a result of their segregation. The mechanism explained above is consistent with the morphological transition from the gyroid to the lamellar phase, and that from the spherical to the cylindrical phase during the curing process observed in the experiment [14].

In the following, we show that the above explanation is confirmed by our DPD simulations. First, we verify whether our simple cross-linking reaction scheme works. Figure 5 shows the temporal change in the ratio of the number of unreacted C-monomers to the total number of C monomers in the system $\rho_{\mathrm{epoxy}}(N = 1)$ during the cross-linking reactions for the case of initial cylindrical phase. In our scheme, the smaller the value of p_c is, the slower the number of unreacted monomers decreases. In addition, when the product of μ^{-1} and p_c is kept constant, $\rho_{\mathrm{epoxy}}(N = 1)$ decreased similarly. We use $\mu = 100$ throughout our study.

To observe the reaction-induced morphological transitions during the cross-linking reaction, we prepare the cylindrical phase as the initial condition. We did not observe the morphological transition when we prepared the lamellar phase as the initial condition (not shown). In our study, three different cases are shown: (i) the moderate cross-linking reaction with $p_c = 0.01$, (ii) the slow cross-linking reaction with $p_c = 0.0001$, and (iii) the rapid cross-linking reaction with $p_c = 1.0$. This is justified by the following estimation: The relaxation time τ of the chain conformation with $N = 10$ in our system is roughly estimated as $\tau \sim 100$.[23] Now we define the reaction rate, i.e., the occurrence probability of the reaction during the unit time $p_{c,\mathrm{unit}} = p_c/(\mu\delta t)$ according to the relation shown in Fig. 5. We can regard $p_{c,\mathrm{unit}}$ as a reciprocal of the characteristic time for the growth of the cross-linking network, and then a dimensionless constant $\tau p_{c,\mathrm{unit}}$ gives $16, 0.16$, and 0.0016 for $p_c = 1.0, 0.01$, and 0.0001, respectively. Therefore, if $\tau p_{c,\mathrm{unit}} \sim 1$, the growth of the cross-linking network is on the same order of the relaxation of the chain, which corresponds the case (i). For the case of $\tau p_{c,\mathrm{unit}} \ll 1 (\gg 1)$, the network growth is much slower (faster) than the relaxation of the chain, which corresponds to the case (ii)((iii)). We discuss the case (iii) in the next subsection.

Figure 6 shows the morphological transition in the case (i). In

this case, the cylindrical domains quickly transform into the irregular lamellar structures. On the other hand, when the reaction probability is low as in the case (ii), an ordered lamellar structure appears as shown in Fig. 7. We provide movies of temporal evolutions of domain morphologies in each case as a supplemental material. In the provided movies, the reactive C-monomers are not shown for visibility of domains formed by diblock copolymers. It should be noted that these morphological transitions occur even if the mixing of the A-block of the diblock copolymer and the reactive C monomers is athermal. These morphological transitions can be purely caused by the decrease in the translational entropy of reactive monomers owing to the cross-linking reactions, even if there is no repulsive interaction among particles. In the case where the mixing of the A-block of the block copolymer and the reactive C monomer is not athermal, the partial compatibility may cause a nontrivial change to the result[39], which is beyond the scope of this study.

Figure 8 shows the instantaneous one-dimensional density profiles for each type of monomer. To calculate the continuous density distribution for each type of monomer from their coordinates, we use the extrapolation method, in which the density distributions on lattice points are calculated by the linear extrapolation function

$$\rho(x) = \begin{cases} 0, & x \le x_p - r_c \\ 1.0 - (x_p - x)/r_c, & x_p - r_c < x \le x_p \\ 1.0 - (x - x_p)/r_c, & x_p < x \le x_p + r_c \\ 0 & x > x_p + r_c, \end{cases} \tag{14}$$

where x_p is the position of the particle. Before the cross-linking reaction, A-blocks of diblock copolymer and reactive C-monomers do not segregate as shown in Fig. 8(a), since their mixing is athermal. After the cross-linking reaction, A-monomers and the cross-linking networks formed by the C-monomers segregate due to the polymerization as shown in Fig. 8(b).

4.2 Domain spacing by cross-linking network

In this subsection, we discuss the morphological behavior after the cross-linking reaction with $p_c = 1.0$, which we mentioned as the case (iii) in the last subsection. When the formation of the cross-linking network is fast, we observe that the initial morphologies are preserved, since the cross-linking network does not allow the cylindrical domains to deform and reconnect. Figure 9 shows the cylindrical phase before and after the cross-linking reaction takes place. After the cross-linking reaction, the A-blocks of the diblock copolymer strongly segregate from the network matrix since the monomers lose their translational entropy due to the cross-linking reaction. In the experiment of Lipic *et al.*[14], when the cross-linking reaction proceeds while the cylindrical domain morphology is preserved, a change in a domain spacing (spacing between neighboring cylinders) is observed. To confirm the change in the domain spacing after the cross-linking reaction in DPD simulation, we estimate the most stable system size of the simulation box by measuring the anisotropy of the pressure. In order to measure anisotropy of the pressure, we first prepare an

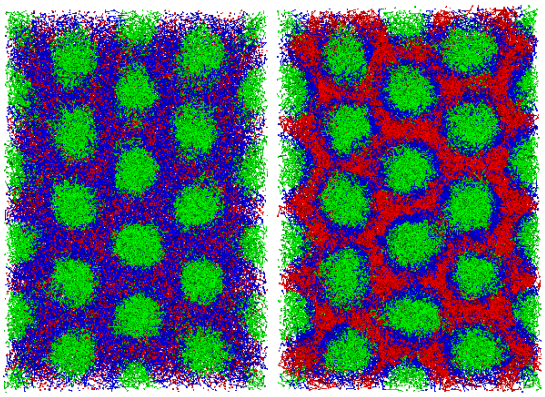

Fig. 9 (Left): A cylindrical phase as the initial domain morphology at $t = 0$. (Right): The cylindrical domains in the cross-linking networks at $t = 4800$. The deformation of the cylindrical domains is hindered by the cross-linking network, and thus the cylindrical phase is preserved. It should be noted that both of particles and bonds are visualized here.

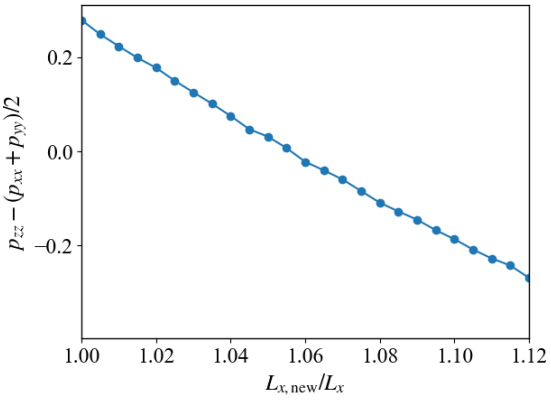

Fig. 10 Anisotropy in the stress tensor due to the anisotropic domain morphology as a function of the ratio of the resized system size to the original system size. When the anisotropy is zero, the isotropic true equilibrium state is realized.

equilibrium system where $P_{xx} = P_{yy} = P_{zz}$ is satisfied, and then we measure the pressure difference $P_{zz} - (P_{xx} + P_{yy})/2$ after the cross-linking reaction by changing the system size in the parallel direction to the original cylindrical domains. After such a preparation, we adjust the system sizes appropriately to find the isotropic equilibrium state.

Figure 10 shows the pressure difference after the cross-linking reaction. The simulations are performed by changing the system size L_x in the direction parallel to the cylindrical axis, where the total volume of the simulation box is kept constant. The horizontal axis of Fig. 10 represents the ratio of the simulated system size $L_{x,\mathrm{new}}$ to its original size before the cross-kinking reaction occurs, L_x. The vertical axis shows the anisotropy in the pressure tensor, whose zero value means that the system realizes an isotropic state with the deformed simulation box with $L_{x,\mathrm{new}}/L_x$. When this ratio is unity, the anisotropy of the pressure tensor deviates from zero, which indicates that the structural anisotropy emerges due to the cross-linking reaction. To recover the isotropy of the pres-

sure, we enlarge the system size L_x and L_y, and simultaneously reduce L_z to keep the system volume constant. By this procedure, we obtain a state where an isotropic pressure is realized when $L_{x,\mathrm{new}} \approx 1.055 L_x$. This suggests that the system expands in the plane spanned by x and y axes, that is, the plane perpendicular to the cylindrical axis, and shrinks along the direction parallel to the cylindrical axis (z-axis) during the cross-linking reaction. This behavior originates from the segregation between the B-block of the diblock copolymers and the monomers driven by the cross-linking reaction. When the cross-linking reaction occurs, the segregation becomes stronger since the monomers lose their translational entropy for mixing. This segregation causes an effective repulsive interaction between cylindrical domains. The enhancement of this immiscibility between the two phases inside and outside the cylindrical domains leads to an increase in the domain periodicity in the xy-plane. However, such a repulsion of the domains is compensated by the elastic force of the cross-linking network formed from the monomers. A balance between the repulsion force and the elastic attractive force determines the new equilibrium state. The similar behavior was observed in the experiment [13].

4.3 Morphological order for slow reactions

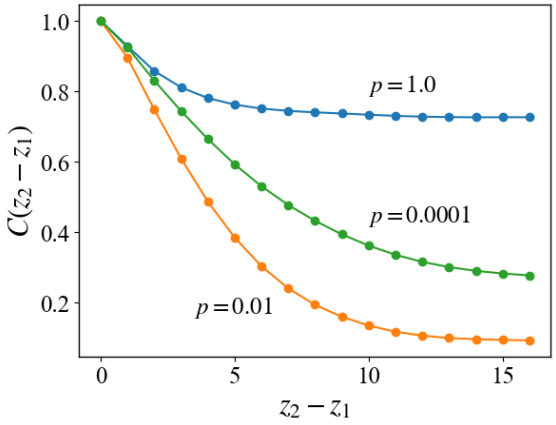

Fig. 11 Correlation function $C(z)$ of the density profiles in the planes normal to the cylindrical axis. For the case of $p_c = 1$, the initial microphase-separated structures are preserved and the correlation along z-axis is kept high. For the case of $p_c = 0.01$, the correlation becomes much lower, which indicates that the lamellar structure is irregular along z-axis. For the case of $p_c = 0.0001$, the correlation is higher than that for the case of $p_c = 0.01$, which indicates that the slower cross-linking reaction keeps the regularity of the morphologies after the cross-linking reaction.

Here we discuss the dependence of the ordering kinetics on the reaction probability. In the previous subsections, we show the dynamics of morphological transition from cylindrical structure to the lamellar structure during the cross-linking reaction, and we observe that the reaction probability p_c determines whether the system transforms into the regular (well-ordered) or irregular lamellar structure. To evaluate the dependence of the ordering of the domain structure on the reaction probability p_c, we define the

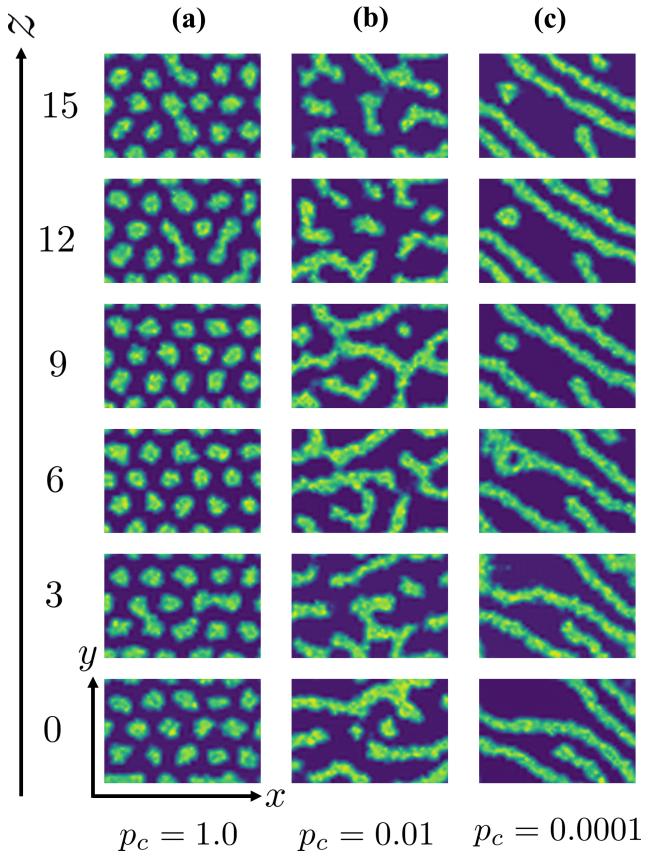

Fig. 12 Examples of two-dimensional crosssections of the density distribution at some values of z-coordinate for different reaction probabilities. (a) In the case of the rapid reaction with $p_c = 1.0$, the preserved cylindrical domains regularly arrange. (b) In the case of the reaction with the moderate rate $p_c = 0.01$, the crosssections nearby ($|\Delta z| \sim 3$) share a weak resemblance. (c) In the case of the slow reaction with $p_c = 0.0001$, the crosssections at a large distance ($|\Delta z| \sim 6$) are similar.

following correlation function:

$$C(z_1 - z_2) = \langle \int dxdy(\rho(x,y;z_1) - \bar{\rho}(z_1))(\rho(x,y;z_2) - \bar{\rho}(z_2))\rangle, \quad (15)$$

where $\langle \cdots \rangle$ represents the ensemble average over 10 different simulations for a given reaction probability p_c. The three-dimensional density is defined as $\rho(\mathbf{r}) = \rho(x)\rho(y)\rho(z)$ by using Eq.(14). The correlation function defined in Eq.(15) represents the correlation or similarity of two-dimensional density distributions $\rho(x,y;z)$ with the distance $|z_1 - z_2|$. Figure 11 shows the correlation function according to Eq. (15) for the case of each reaction probability, and Fig. 12 shows the examples of the two-dimensional crosssections of the density distributions along the z-direction for each case.

For the case of $p_c = 1$, which corresponds to the case of Fig. 9, two-dimensional structure keeps the high correlation even for the two-dimensional cross-sections far from each other. The cross-linking network formed under the rapid reaction condition, as mentioned in the last subsection, does not allow the cylindrical domains to deform, and the cylindrical domains are preserved by the surrounding networks, as you can see in the Fig. 12(a). This

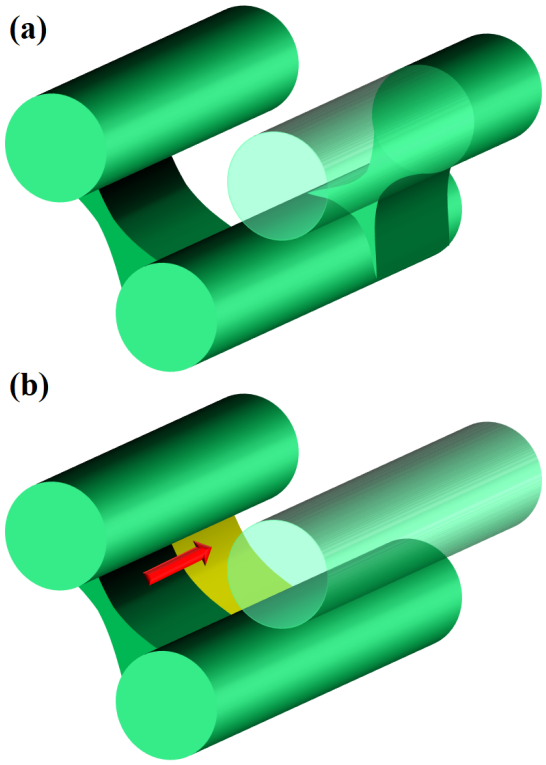

Fig. 13 Schematic pictures of the process of the connection between cylinders. (a) In the case of the moderate reaction rate, cylinders are randomly connected by bridging domains, as in the case of the spinodal decomposition. (b) In the case of the slow reaction rate, the nucleation and growth process takes place, where a bridging domain between nearby cylinders is nucleated and grows along the cylinder swiftly.

leads to the high correlation along the z-axis in the same manner as in the equilibrium state.

For the cases of $p_c = 0.01$ and 0.0001, the formations of cross-linking networks are rather slow that the domains can deform and reconnect with each other, leading to the reaction-induced cylinder-lamellar transition. As a result, the morphological transitions from the cylinder to the lamellar are observed for both cases with $p_c = 0.01$ and $p_c = 0.0001$. However, the case with $p_c = 0.0001$ shows higher correlations than the case with $p_c = 0.01$. This result suggests that the ordering in the lamellar domains is promoted when the reaction is slow ($p_c = 0.0001$), while the lamellar domains are irregular when the reaction probability is moderate ($p_c = 0.01$), as you see in Figs. 12(b) and (c). These different behaviors are similar to those of reaction-induced viscoelastic phase separation[40]. Figure 13 depicts the intuitive explanation of the two processes of the connections of cylinders during cross-linking reactions. In the case of the moderate reaction rate, reactive monomers surrounding the cylindrical domains form the cross-linking network, whereby the translational entropy decreases rapidly and uniformly along the cylindrical domains, which causes an instability of the domain morphology similar to the spinodal decomposition (Fig. 13(a)). This leads to the random connections between cylindrical domains, where a given domain connects to some neighboring domains along the cylindrical axis. These random connections result in the irregular lamellar structures in the case of moderate reaction probability. On the other hand, in the case of the slow reaction rate, the formation of the cross-linking networks proceeds gradually. When the cross-linking networks develop locally, a rung between neighboring cylinders is formed by an activation process due to thermal fluctuation. Once a rung is formed, it expands quickly along the cylindrical domain, leading to a formation of sheet-like domains.(Fig. 13(b)) As a result, a cylindrical domain is connected with a fewer rung to its neighboring cylinders in a regular manner compared to the case of the moderate reaction probability.

5 Conclusion

In the present study, we perform the DPD simulation to investigate the reaction-induced morphological transitions in a blend of symmetric diblock copolymers and reactive monomers. To prepare the true equilibrium state as an appropriate initial conditions for the DPD simulations, we perform the SCFT calculation combined with the density-biased Monte Carlo method. Our SCFT simulation predicts the phase diagram that is consistent with the experimental results in the intermediate segregation regime with the incompatibility parameter χN. The experimentally observed morphological transitions during the cross-linking reaction from the microphase-separated structures with a high curvature to that with a lower curvature are well reproduced in our DPD simulation. Moreover, the experimental result of the increase in the domain spacing after the cross-linking reaction is successfully reproduced.

By simulating the cross-linking reactions with various reaction probabilities, we find that the morphological transitions undergo two different mechanisms, that is, the nucleation and growth in the case of slow reaction and the spinodal decomposition in the case of moderate reaction. These mechanisms deeply relate to the reaction-induced instability and to the spatial arrangement and regularity of the microphase-separated domains after the cross-linking reaction. Our simulations suggest a possible understanding of the dynamical pathway of the transition in domain morphologies, which contributes to applications in the nanotechnology engineering.

Conflicts of interest

There are no conflicts to declare.

Acknowledgement

Financial support from Cross-ministerial Strategic Innovation Promotion Program (SIP) “Materials Integration for Revolutionary Design System of Structural Materials” (Funding agency: JST) is gratefully acknowledged.

References

1 A. F. Yee and R. A. Pearson, J. Mater. Sci., 1986, **21**, 2462–2474.
2 R. A. Pearson and A. F. Yee, J. Mater. Sci., 1986, **21**, 2475–2488.
3 R. A. Pearson and A. F. Yee, J. Mater. Sci., 1989, **24**, 2571–2580.

4 A. Allaoui, Compos. Sci. Technol., 2002, **62**, 1993–1998.
5 Z. Ahmadi, Prog. Org. Coat., 2019, **135**, 449–453.
6 T. Okabe, T. Takehara, K. Inose, N. Hirano, M. Nishikawa and T. Uehara, Polymer, 2013, **54**, 4660–4668.
7 B. A. Alshammari, M. S. Alsuhybani, A. M. Almushaikeh, B. M. Alotaibi, A. M. Alenad, N. B. Alqahtani and A. G. Alharbi, Polymers, 2021, **13**, 2474.
8 J. Wu, Y. S. Thio and F. S. Bates, J. Polym. Sci. B: Polym. Phys., 2005, **43**, 1950–1965.
9 E. Serrano, M. D. Martin, A. Tercjak, J. A. Pomposo, D. Mecerreyes and I. Mondragon, Macromol. Rapid Commun., 2005, **26**, 982–985.
10 L. Ruiz-Pérez, G. J. Royston, J. P. A. Fairclough and A. J. Ryan, Polymer, 2008, **49**, 4475–4488.
11 H. Kishi, Y. Kunimitsu, J. Imade, S. Oshita, Y. Morishita and M. Asada, Polymer, 2011, **52**, 760–768.
12 H. Kishi, Y. Kunimitsu, Y. Nakashima, T. Abe, J. Imade, S. Oshita, Y. Morishita and M. Asada, EXPRESS Polym. Lett., 2015, **9**, 23–35.
13 M. A. Hillmyer, P. M. Lipic, D. A. Hajduk, K. Almdal and F. S. Bates, J. Am. Chem. Soc., 1997, **119**, 2749–2750.
14 P. M. Lipic, F. S. Bates and M. A. Hillmyer, J. Am. Chem. Soc., 1998, **120**, 8963–8970.
15 K. Yamanaka and T. Inoue, Polymer, 1989, **30**, 662–667.
16 K. Yamanaka, Y. Takagi and T. Inoue, Polymer, 1989, **30**, 1839–1844.
17 H. Liu, H.-J. Qian, Y. Zhao and Z.-Y. Lu, J. Chem. Phys., 2007, **127**, 144903.
18 A. A. Gavrilov, D. V. Guseva, Y. V. Kudryavtsev, P. G. Khalatur and A. V. Chertovich, Polym. Sci. Ser. A, 2011, **53**, 1207–1216.
19 S. Thomas, M. Alberts, M. M. Henry, C. E. Estridge and E. Jankowski, J. Theor. Comput. Chem., 2018, **17**, 1840005.
20 C. Li and A. Strachan, Polymer, 2018, **149**, 30–38.
21 P. J. Hoogerbrugge and J. M. V. A. Koelman, Europhys. Lett., 1992, **19**, 155–160.
22 R. D. Groot and P. B. Warren, J. Chem. Phys., 1997, **107**, 4423–4435.
23 R. D. Groot and T. J. Madden, J. Chem. Phys., 1998, **108**, 8713–8724.
24 G. Kacar, E. A. J. F. Peters and G. de With, Soft Matter, 2013, **9**, 5785.
25 M. Langeloth, T. Sugii, M. C. Böhm and F. Müller-Plathe, J. Chem. Phys., 2015, **143**, 243158.
26 Y. Kawagoe, G. Kikugawa, K. Shirasu and T. Okabe, Soft Matter, 2021, **17**, 6707–6717.
27 T. Aoyagi, F. Sawa, T. Shoji, H. Fukunaga, J. ichi Takimoto and M. Doi, Comput. Phys. Commun., 2002, **145**, 267–279.
28 http://octa.jp/.
29 Nanostructured Soft Matter, ed. A. V. Zvelindovsky, Springer Netherlands, 2007.
30 M. W. Matsen, J. Chem. Phys., 2020, **152**, 110901.
31 M. W. Matsen, Phys. Rev. Lett., 1995, **74**, 4225–4228.
32 M. W. Matsen, Macromolecules, 1995, **28**, 5765–5773.
33 A. N. Semenov, Macromolecules, 1993, **26**, 2273–2281.
34 A. E. Likhtman and A. N. Semenov, Macromolecules, 1997, **30**, 7273–7278.
35 M. W. Matsen, Macromolecules, 2003, **36**, 9647–9657.
36 A. N. Semenov, Sov. Phys. JETP, 1985, **61**, 733–742.
37 E. W. Cochran, C. J. Garcia-Cervera and G. H. Fredrickson, Macromolecules, 2006, **39**, 2449–2451.
38 W. Liu, H.-J. Qian, Z.-Y. Lu, Z.-S. Li and C.-C. Sun, Phys. Rev. E, 2006, **74**, 021802.
39 A. A. Gavrilov and A. V. Chertovich, Macromolecules, 2017, **50**, 4677–4685.
40 Y. Oya, G. Kikugawa, T. Okabe and T. Kawakatsu, Adv. Theory Simul., 2022, **5**, 2100385.